JOURNAL OF APPLIED ELECTROCHEMISTRY **26** (1996) 451–457

Silver electrocrystallization from a nonpolluting aqueous leaching solution containing ammonia and chloride

A. SERRUYA, B. R. SCHARIFKER*

Universidad Simón Bolívar, Departamento de Química, Apartado 89000, Caracas 1080-A, Venezuela

I. GONZÁLEZ, M. T. OROPEZA, M. PALOMAR-PARDAVÉ

Universidad Autónoma Metropolitana-Iztapalapa, Departamento de Química, Apartado Postal 55-534, C.P. 09340 Mexico D.F., Mexico

Received 25 July 1995; revised 14 September 1995

Silver electrocrystallization from aqueous solutions at pH 11, pCl 0 and $pNH_3 - 0.2$, where $Ag(NH_3)_2^+$ is the dominant Ag(I) species, has been studied. In spite of the complexities of this medium, the experimental results can be satisfactorily described in terms of multiple nucleation and diffusion-controlled growth of hemispherical nuclei. Nucleation rates, A, and number densities of active sites on the electrode surface, N_0, were determined from potentiostatic current transients as a function of overpotential. Saturation number densities of silver nuclei on the electrode surface obtained from the A and N_0 values were found to be in excellent agreement with those obtained from the direct, microscopic observation of the electrode surface. Spatial distributions of nuclei were also analysed for silver electrodeposited at different potentials. It was found that nuclei were uniformly distributed when electrodeposited at low overpotentials, whereas inhibition of nucleation close to already established nuclei occurred at higher overpotentials. From the change of the true nucleation rate with overpotential, it was found that the critical nucleus is formed by a single atom within the −100 to −300 mV overpotential range.

1. Introduction

The early stages of electrochemical phase formation at constant potential onto foreign substrates have been considered theoretically by several authors [1–13], who have described the functional forms of the current transients, which depend on the geometry of nuclei and the rate-limiting step in the process. In the case of diffusion-controlled growth of hemispherical nuclei, Scharifker and Mostany [9] have proposed a model to estimate, from potentiostatic current transients, the true nucleation rate constant per site, A, and the number density of active sites on the surface, N_0, separated from their product, AN_0, also known as the steady state nucleation rate, I_{SS}, which is usually obtained from microscopic counting of the number of nuclei appearing on the electrode surface at a given overpotential as a function of time. Thus this model offers advantages in the study of electrocrystallization in the classical and atomistic [14–16] limits.

Most often, electrocrystallization theories have been tested using simple systems [17–26], where the dominant chemical species of the electrodepositing ion shows a first coordination sphere comprised of solvent molecules, and where the supporting electrolyte of choice has been a strong electrolyte, weakly adsorbing on the electrode or nucleus surfaces, such as potassium nitrate. In this work we have studied the electrocrystallization of silver in a considerably more intricate system, namely an alkaline leaching bath in which ammonia and chloride occur at high concentrations, and where the silver diammonia complex is the dominant species. This bath has been shown to be efficient in the extraction of silver [27–30] with the further advantage of being more environmentally friendly than the traditional cyanide bath. Information on the early stages of silver electrocrystallization from ammonia–chloride solutions may contribute to obtaining better deposits, as well as to encourage the use of this novel bath with potential environmental benefit.

2. Experimental details

A two-compartment, three-electrode cell was used throughout. The bottom of the main compartment was an optically flat window so as to observe *in situ* the working electrode surface with the aid of a COHU 4815 monochrome video camera, connected to a metallographic microscope and a digital signal processing system to acquire and analyse images of the electrode surface displayed on a TV monitor.

The working electrode was a vitreous carbon disc (Electrosynthesis, GC-30) of 7.07×10^{-2} cm^2 exposed area, sealed to glass and polished with several

* Author to whom correspondence should be addressed.

0021-891X

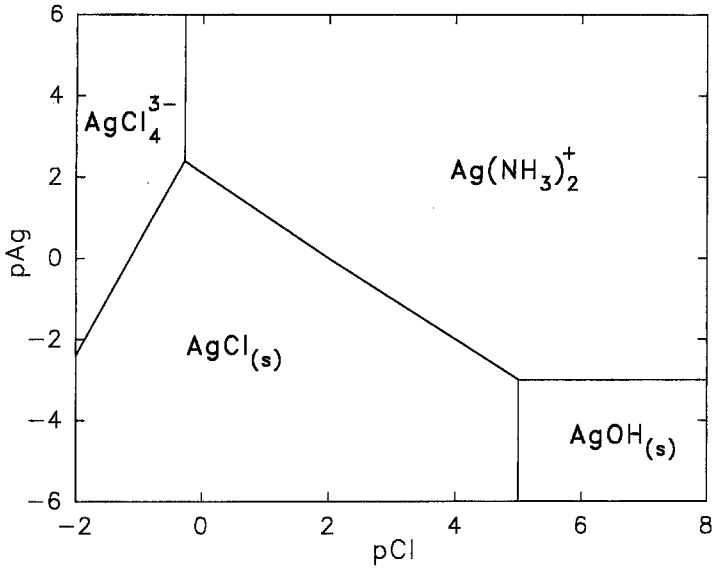

Fig. 1. Diagram of dominant soluble and insoluble silver species in aqueous solution at varying Ag^+ and Cl^- concentrations, pH 11 and $pNH_3 - 0.2$.

grades of alumina down to 0.05 μm. The secondary electrode was a platinum ring placed near the bottom of the cell, around the working electrode, which was located at about 1 cm of the optical flat. The reference electrode was a silver wire, immersed in the same working solution, but in a separate compartment, connected to the main through a Luggin capillary. The working electrode potential was controlled with an EG&G PAR model 273 potentiostat/galvanostat, connected to a PC through an IEEE-488 interface.

Silver electrocrystallization was studied from aqueous 2.2 mM $AgNO_3$ solutions, containing also 1 M NaCl and 1.6 M NH_3, pH 11, conditions under which the $Ag(NH_3)_2^+Cl^-$ species is formed [28]. All solutions were prepared with analytical grade reagents and ultrafiltered distilled water of 17.6 MΩ cm resistivity.

The kinetics of nucleation was studied with single potential steps to cathodic overpotentials between −100 and −300 mV, at 20 mV intervals. Current transients were recorded and an image with the nuclei electrodeposited on the electrode surface was acquired at the end of each experiment. Nuclei were dissolved between experiments immersing the electrode surface successively in (i) a 1% NaCN and 6% hydrogen peroxide solution, (ii) distilled water, (iii) ammonium hydroxide solution, pH 11, and finally (iv) distilled water, before replacing the working electrode in the electrochemical cell.

2.1. *Image analysis*

The size of the segment of the electrode surface under study was determined by calibration with a 1 mm ruler, with subdivisions at 10 μm. Regions of 1.00×10^{-4} to 4.00×10^{-4} cm^2 were analysed, the larger areas were necessary for experiments in which a low number density of nuclei were produced on the surface. The location of each nucleus within the region under study was determined with the help of a cursor on the TV monitor. The corresponding coordinates were later used to obtain the nearest neighbour distribution functions [42] and the saturation number densities of nuclei, $N_{s,m}$, on the electrode surface.

2.2. *Analysis of current transient data*

The nucleation rate, A, and the number density of active sites, N_0, were obtained from the potentiostatic current maximum [9]. The values of A and N_0 thus obtained were used to estimate saturation nuclear number densities from current transients, $N_{s,t}$, which were later compared with those obtained from analysis of microscope images, $N_{s,m}$.

3. Results and discussion

3.1. *Electrodepositing species*

The dominant silver (I) species in the ammonia–chloride leaching bath used in this work [30] was determined by thermodynamic analysis according to the formalism introduced by Rojas *et al.* [31–35], from which the diagram shown in Fig. 1, for pH 11 and $pNH_3 - 0.2$, was obtained. Introducing the silver and chloride concentrations relevant to this work, pAg 2.66 and pCl 0, it follows that in spite of the relatively large chloride concentration, the dominant silver species in solution is $Ag(NH_3)_2^+$.

3.2. *Potentiostatic current transients*

A family of potentiostatic current transients recorded during silver electrodeposition from the leaching solution studied here is shown in Fig. 2. The transients show the characteristic shape predicted in [9], that is, rising currents due to the birth and growth of nuclei, followed by decaying currents that at sufficiently negative overpotentials, approach asymptotically the well known Cottrell equation.

3.3. *Determination of the diffusion coefficient*

Analysis of current transients such as those shown in

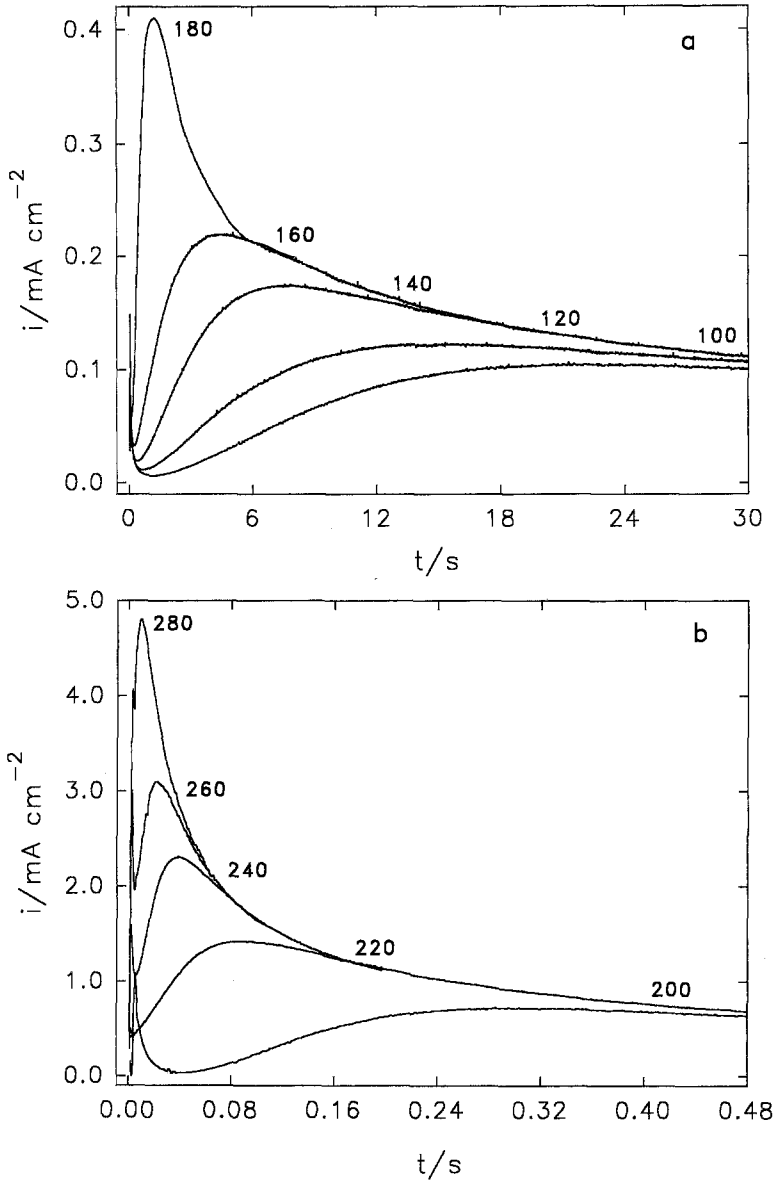

Fig. 2. Potentiostatic current transients for silver electrocrystallization on to vitreous carbon from 2.2 mM $AgNO_3$ + 1 M NaCl + 1.6 M NH_3 aqueous solution, pH 11, at the overpotentials indicated: (a) 100 to 180, and (b) 200 to 280 mV.

Fig. 2 requires knowledge of the diffusion coefficient of the electrodepositing species. The diffusion coefficient of the $Ag(NH_3)_2^+$ ion was determined through various electrochemical techniques: chronoamperometric measurements at stationary electrode and high overpotential, steady state current at rotating disc electrode, polarography at dropping mercury electrode, and conductivity measurements at 1 kHz with platinized platinum electrodes. The diffusion coefficient used for analysis of transients was an average of the values obtained with these techniques, $2.2 \times 10^{-5}\,cm^2\,s^{-1}$, which is close to that obtained from conductivity and chronoamperometric measurements and, as described below, leads to the required solutions of the system of equations used for interpretation of the transients.

3.4. *Analysis of transients*

As suggested by Milchev [21], given that analysis of each of the transients is carried out from a single experimental pair of values obtained from its current maximum, it is desirable to verify whether the equation used describes the whole of the experiment. This might be done comparing experimental $(i/i_m)^2$ against t/t_m plots with those obtained from the theoretical expression

$$\left(\frac{i}{i_m}\right)^2 = \left(\frac{t_m}{t}\right) \times \frac{\{1-\exp[-xt/t_m + a(1-\exp(-xt/t_m))]\}^2}{\{1-\exp[-x+a(1-\exp(-x/a))]\}^2} \quad (1)$$

where

$$x = N_0\pi D(8\pi cM/\rho)^2 t_m \quad (2)$$

$$a = N_0\pi D(8\pi cM/\rho)^2/A \quad (3)$$

In Equation 1, i_m and t_m are the coordinates of the experimental current transient maximum, and in Equations 2 and 3 D is the diffusion coefficient, c is the bulk concentration, and zF is the molar charge of the electrodepositing species, M and ρ are the molecular weight and density of the deposited materials respectively, A is the nucleation rate constant per site and N_0 is the number density of active sites. Such a comparison between experimental and theoretical transients is shown in Fig. 3.

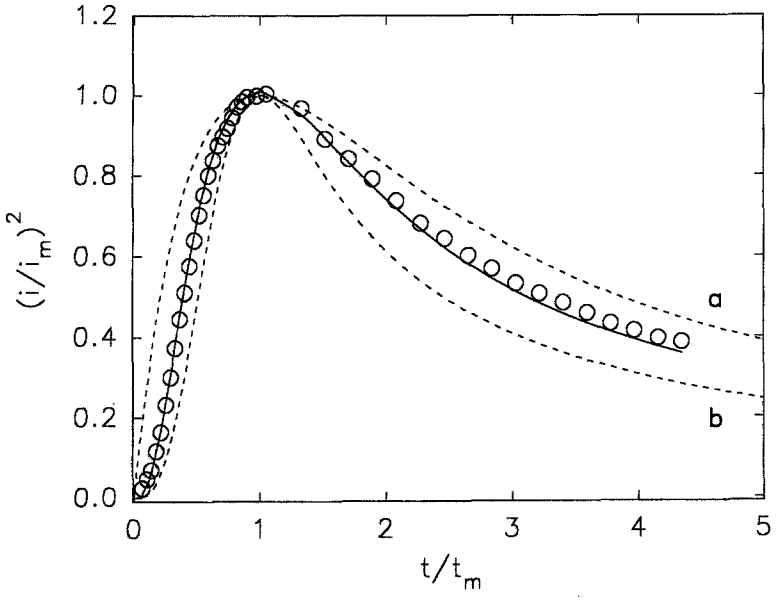

Fig. 3. Comparison of experimental transient recorded during silver electrocrystallization at 160 mV overpotential (○), and theoretical transient (—) according to Equation 4, with $D = 2.2 \times 10^{-5}\,cm^2\,s^{-1}$, $A = 1.06\,s^{-1}$ and $N_0 = 2.77 \times 10^5\,cm^{-2}$. The dashed lines show the theoretical transients corresponding to the (a) 'instantaneous' and (b) 'progressive' limits.

Once shown that the theoretical model describes satisfactorily the entire transient, the relevant information can be obtained from the current and time corresponding to the potentiostatic maximum. An important aspect of the model developed in [9] is that it is not necessary to classify *a priori* nucleation as either instantaneous or progressive [7, 8], since these forms appear as limiting cases. Distinction between instantaneous and progressive nucleation is nevertheless still common in the literature [35–41].

The time dependent current is therefore given by Equation 4 [9]:

$$i(t) = \left(\frac{zFD^{1/2}c}{\pi^{1/2}t^{1/2}}\right) \times (1 - \exp\{-N_0\pi kD[t - A^{-1}(1 - e^{-At})]\}) \quad (4)$$

with $k = (8\pi cM/\rho)^{1/2}$

The current maximum and its corresponding time define the following pair of transcendental nonlinear equations:

$$\ln(1 - i_m t_m^{1/2}/a) + x - a(1 - e^{-x/a}) = 0 \quad (5a)$$

$$\ln[1 + 2x(1 - e^{-x/a})] - x + a(1 - e^{-x/a}) = 0 \quad (5b)$$

from which N_0 and A may be obtained simultaneously from single pulse potentiostatic experiments. Here we resolved the system of equations (5) numerically [9], using the routine EQ001 developed by Mostany [42]*.

3.5. *Micrographic analysis*

Results from interpretation of transients as outlined above were compared with analysis of microscope images of the electrode surface, acquired *in situ* immediately after the electrode potential perturbation. From these images, the saturation number

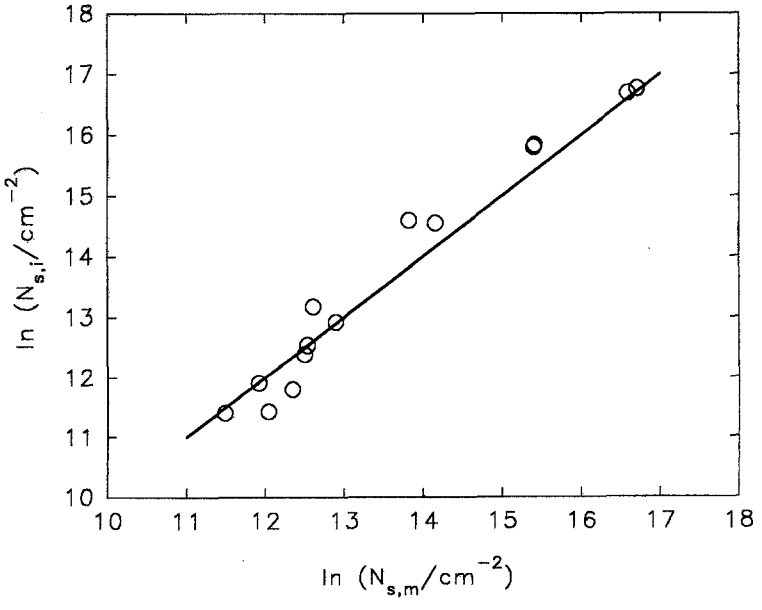

Fig. 4. Number density of nuclei derived from analysis of current transients, $N_{s,i}$, as a function of the number density of nuclei obtained from microscope images, $N_{s,m}$. The line represents the linear correlation with unity slope.

*Copies of the routine may be obtained from Dr. J. Mostany, Departmento de Química, Universidad Simón Bolívar, Apartado 8900, Caracas 1080-A, Venezuela.

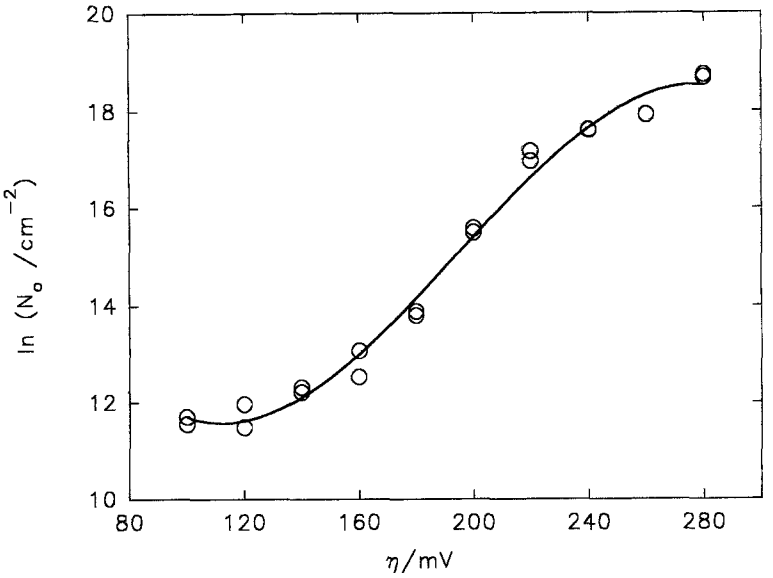

Fig. 5. Number density of active sites for nucleation as a function of the overpotential for silver deposition.

density of nuclei on the surface ($N_{s,m}$) was directly obtained. Further details about the methods used for image analysis have been described elsewhere [43, 44]. The saturation nuclear number densities thus obtained at the various potentials were compared with those deduced from the transients, $N_{s,i}$, with the following expression, [8]

$$N_{s,i} = (AN_0/2kD)^{1/2} \quad (6)$$

Figure 4 shows a comparison between the values of $N_{s,i}$, deduced from interpretation of chronoamperometric data, and $N_{s,m}$, obtained directly from microscope images of the electrode surface acquired after potential steps. The excellent linear correlation with slope one validates the method used for the analysis of transients in this complex solution, and the values of A and N_0 obtained from it.

3.6. *Variation of N_0 with overpotential*

Figure 5 shows the number density of active sites as a function of the overpotential for silver deposition. N_0 increases with the cathodic overpotential, from around 2×10^5 cm^{-2} at low overpotentials to about 7×10^7 cm^{-2} at overpotentials as high as 280 mV. Even at such high overpotential the number density of nuclei is over seven orders of magnitude lower than the atomic density of the surface, as has been pointed out for other cases of metal deposition onto vitreous carbon surfaces [44].

3.7. *Overpotential dependence of A*

Figure 6 shows the exponential increase of the nucleation rate per site, A, with the overpotential. Assuming a transfer coefficient of 1/2, the slope of the plot of $\ln(A)$ against η [14, 15] indicates that the number of atoms in the critical cluster is one atom throughout the potential range, and that supercritical nuclei develop by direct discharge and incorporation of ions from solution, without involving adatoms. During silver electrocrystallization on vitreous carbon from potassium nitrate solutions, Milchev *et al.* [18, 19] have found that the critical size decreased from 1 to 0 atoms as the overpotential increased. The difference with respect to the result obtained

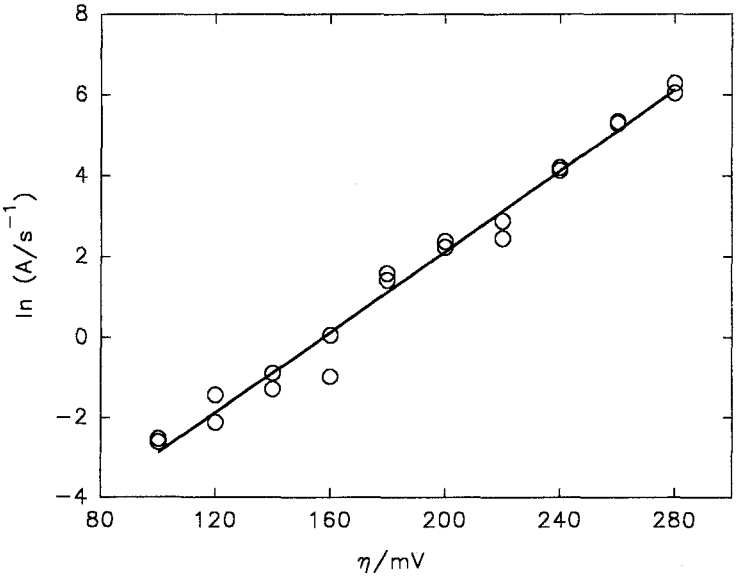

Fig. 6. Nucleation rate per site as a function of the overpotential for silver deposition.

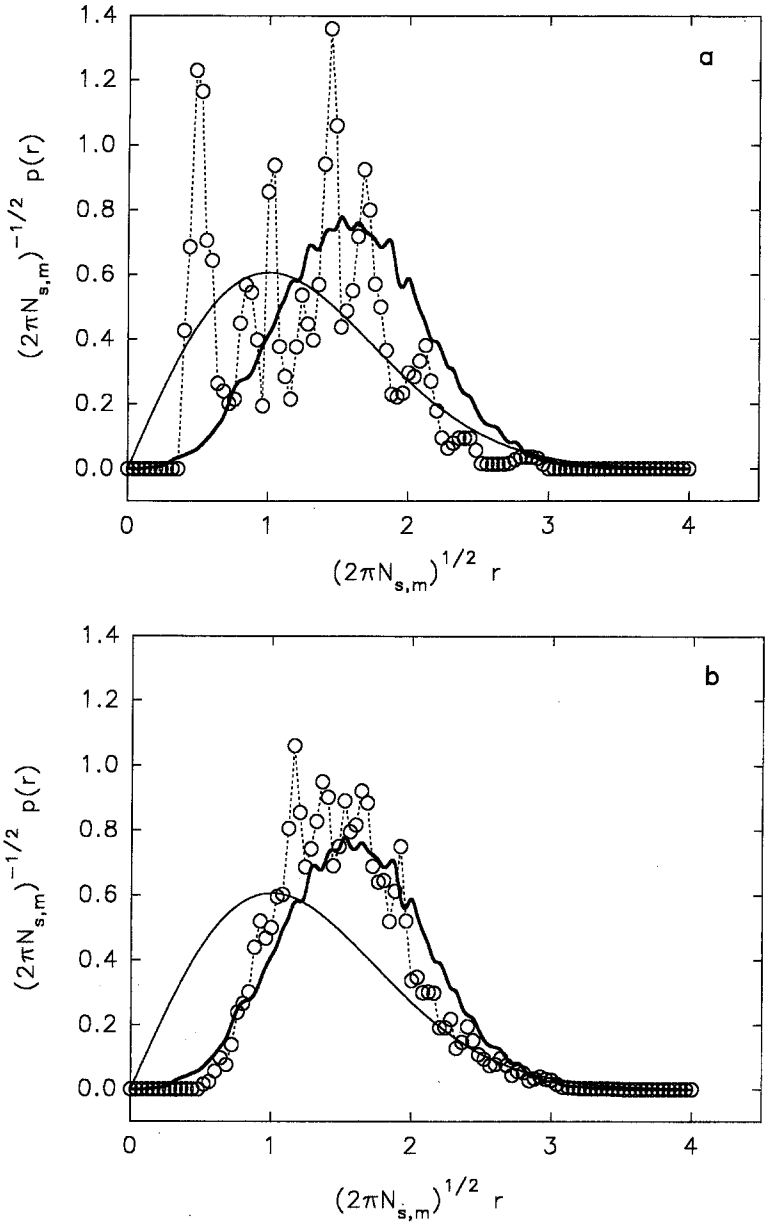

Fig. 7. Nearest neighbour distribution functions obtained from analysis of microscope images of the electrode surface after nucleation at (a) 100 and (b) 200 mV. Experimental data (– – O – –), uniform distribution (——), computer simulated distribution considering nucleation exclusion zones around nuclei (▬▬).

here might be due to the presence of ammonia molecules in the silver coordination sphere, as well as the possible adsorption of chloride ions at the interphase. To clarify these aspects, in subsequent papers we will address the effects of the coordination sphere of the electroactive species, as well as the nature of the supporting electrolyte, upon electrocrystallization mechanisms.

3.8. *Spatial distribution of nuclei*

The birth rate of nuclei on the electrode surface is limited by the availability of active sites [44], which diminishes continuously throughout the nucleation process, either as a result of their conversion into growing nuclei, or due to the reduced activity of the remaining sites caused by the growth of adjacent nuclei.

Inhibition of the nucleation process in the vicinity of growing nuclei not only leads to saturation of their number density, but also affects the spatial distribution of nuclei on the electrode surface. The spatial distribution may be studied by analysis of the distribution of distances between nearest neighbours [45]. Representing this distribution in nondimensional form, the nuclear number density is removed as a parameter in the distribution and the probability density function of the nearest-neighbour distribution only reflects the way nuclei are arranged on the plane, allowing comparison of experimental distributions with theoretical distributions corresponding to hypothetical cases [45] (e.g., like the uniform distribution of particles on the plane, square or hexagonal lattices, and so on).

Analysis of the spatial distribution shows that silver nuclei are uniformly distributed when deposited at low overpotentials, whereas at high overpotential the distribution is affected by exclusion or inhibition of the nucleation process around already established nuclei, up to distances that expand with $t^{1/2}$. Figure 7 shows in reduced coordinates the nearest-neighbour analysis of the spatial distribution; the experimental distributions are presented together with the probability density functions corresponding to points randomly allocated on the surface, and the

results of computer simulations of the nucleation process considering nucleation exclusion zones around nuclei [45]. The plots in Fig. 7 show that short distances between nuclei are avoided when electrocrystallization is carried out at high overpotentials. Similar results have been obtained for the spatial distribution of silver nuclei electrodeposited from nitrate bath [46], as well as in other previously studied systems [43] and is related to the sigmoidal variation of $\ln(N_0)$ with overpotential, cf. Fig. 2, which is likely to be due to distributed nucleation energies over different sites along the surface [45, 47].

It is also of interest to analyse the spatial distribution of electrodeposited nuclei beyond their nearest neighbours, that is, the distances between second, third, ..., *n*th neighbours [48, 49], which provides further insights on the mechanism of the nucleation process [50]. Such an analysis for silver electrocrystallization from baths of diverse composition will be published elsewhere [51].

4. Conclusions

The results show that transient analysis [9] can be used for the study of nucleation in a rather complex system, such as the environmentally friendly leaching bath for silver electrodeposition used here. The predictive capacity of the model used for the interpretation of current transients in relation to the saturation number density of nuclei was supported by the *in situ* micrographic analysis of the electrode surface. The early stages of the electrodeposition of silver from ammonia–chloride leaching bath is dominated by multiple nucleation and hemispherical diffusion-controlled growth of nuclei. Both the nucleation rate constant and the number density of active sites were found to be strongly dependent on the overpotential. Within the framework of the atomistic nucleation theory, it was determined that the critical nucleus comprises one silver atom. The spatial distribution of the electrodeposited nuclei on the electrode surface is uniform at low overpotentials, whereas at high overpotential is affected by zones of reduced nucleation rate around already established nuclei.

Acknowledgements

M. T. Oropeza and M. Palomar gratefully acknowledge CONACYT for research studentships. This work has been carried out under the auspices of CONICIT (Venezuela) and CONACYT (Mexico). We are also grateful to Dr Jorge Mostany for his assistance with the numerical routines used to analyse data throughout this work.

References

[1] H. R. Thirsk and J. A. Harrison, 'A Guide to the Study of Electrode Kinetics', Academic Press, London (1972), chapter 3.
[2] E. Bosco and S. K. Rangarajan, *J. Chem. Soc. Faraday Trans. 1* **77** (1981) 1963.
[3] B. Bhattacharjee and S. K. Rangarajan, *J. Electroanal. Chem.* **302** (1991) 207.
[4] M. Y. Abyaneh and M. Fleischmann, *Electrochim. Acta* **27** (1982) 1513.
[5] E. Bosco and S. K. Rangarajan, *J. Electroanal. Chem.* **134** (1982) 213.
[6] R. G. Barradas, F. C. Benson, S. Fletcher and J. D. Porter, *ibid.* **85** (1977) 55.
[7] G. Guanawardena, G. Hills, I. Montenegro and B. Scharifker, *ibid.* **138** (1982) 225.
[8] B. R. Scharifker and G. Hills, *Electrochim. Acta* **28** (1983) 879.
[9] B. R. Scharifker and J. Mostany, *J. Electroanal. Chem.* **177** (1984) 13.
[10] M. Sluyters-Rehbach, J. H. O. J. Wijenberg, E. Bosco and J. H. Sluyters, *ibid.* **236** (1987) 1.
[11] M. Y. Abyaneh, *Electrochim. Acta* **36** (1991) 727.
[12] F. C. Walsh and M. E. Herron, *J. Phys. D. Appl. Phys.* **24** (1991) 217.
[13] R. Greef, R. Peat, L. M. Peter, D. Pletcher and J. Robinson, 'Instrumental Methods in Electrochemistry', Ellis Horwood, Chichester (1985), chapter 9.
[14] A. Milchev, S. Stoyanov and R. Kaischev, *Thin Solid Films* **22** (1974) 255.
[15] A. Milchev, S. Stoyanov and R. Kaischev, *ibid.* **22** (1974) 267.
[16] D. Walton, *J. Chem. Phys.* **37** (1962) 2182.
[17] A. Milchev and S. Stoyanov, *J. Electroanal. Chem.* **72** (1976) 33.
[18] A. Milchev, E. Vassileva and V. Kertov, *ibid.* **107** (1980) 323.
[19] A. Milchev and E. Vassileva, *ibid.* **107** (1980) 337.
[20] V. Tsakova and A. Milchev, *ibid.* **197** (1986) 359.
[21] *Idem, ibid.* **235** (1987) 237.
[22] *Idem, ibid.* **235** (1987) 249.
[23] G. Guanawardena, G. Hills and I. Montenegro, *ibid.* **138** (1982) 241.
[24] G. Guanawardena, G. Hills, I. Montenegro and B. Scharifker, *ibid.* **138** (1982) 255.
[25] J. Mostany, J. Mozota and B. R. Scharifker, *ibid.* **177** (1984) 25.
[26] A. Milchev, B. Scharifker and G. Hills, *ibid.* **132** (1982) 277.
[27] K. N. Han and M. Xinghui, *US Patent 5 114 687* (1992).
[28] M. T. Oropeza, Thesis UAM-I, Mexico (1991).
[29] M. Palomar, Thesis, UAM-I, Mexico (1992).
[30] M. T. Oropeza, I. González and M. Palomar, 'Non-pollution composition of a leaching bath for precious metal recovery', *Mexican Patent 177 685* (1995).
[31] A. Rojas and I. González, *Analyt. Chim. Acta* **187** (1986) 279.
[32] A. Rojas-Hernández, M. T. Ramírez, J. G. Ibáñez and I. González, *J. Electrochemical Soc.* **138** (1991) 365.
[33] A. Rojas-Hernández, M. T. Ramírez, I. González and J. G. Ibáñez, *Analyt. Chim. Acta* **259** (1992) 95.
[34] A. Rojas-Hernández, M. T. Ramírez and I. González, *ibid.* **278** (1993) 321.
[35] *Idem, ibid.* **278** (1993) 335.
[36] C. Q. Cui, S. P. Jiang and A. C. Tseung, *J. Electrochem. Soc.* **137** (1990) 3418.
[37] R. T. Carlin, W. Crawford and M. Bersch, *ibid.* **139** (1992) 2720.
[38] L. Legrand, A. Tranchan and R. Messina, *ibid.* **141** (1994) 378.
[39] C. L. Hussey and X. Xu, *ibid.* **138** (1991) 1886.
[40] M. Sánchez, C. F. Alonso and J. M. Palacios, *J. Appl. Electrochem.* **23** (1993) 364.
[41] L. Bonou, M. Eyraud and J. Crousier, *ibid.* **24** (1994) 906.
[42] J. Mostany, Memorias del IV Encuentro Nacional de Electroquímica, (edited by B. R. Scharifker, J. J. Suárez and J.L. Mostany), Soc. Venez. Electroquím., Caracos (1991) pp. 17–28.
[43] A. Serruya, J. Mostany and B. R. Scharifker, *J. Chem. Soc. Faraday Trans.* **89** (1993) 255.
[44] B. R. Scharifker, *in* 'Electrochemistry in Transition', (edited by O. J. Murphy *et al.*) Plenum Press, New York (1992), chapter 31.
[45] B. R. Scharifker, J. Mostany and A. Serruya, *Electrochim. Acta* **37** (1992) 2503.
[46] A. Serruya, B. R. Scharifker, M. T. Oropeza and I. González, Resúmenes del XI Congreso Iberoamericano de Electroquímica, Aguas de Lindoia, SP, Brazil (1994) pp. 641–643.
[47] R. L. Deutscher and S. Fletcher, *J. Electroanal. Chem.* **277** (1990) 1.
[48] A. Milchev, W. S. Kruijt, M. Sluyters-Rehbach and J. H. Sluyters, *J. Electroanal. Chem.* **350** (1993) 89.
[49] A. Milchev, *J. Chem. Phys.* **100** (1994) 5160.
[50] J. Mostany, A. Serruya and B. R. Scharifker, *J. Electroanal. Chem.* **383** (1995) 37.
[51] I. González, M. Palomar-Pardavé, M. T. Oropeza, J. Mostany, A. Serruya and B. R. Scharifker, in preparation.